



HAL
open science

Dynamic characterization approach for the investigation of microstructural changes in clay-based materials during firing

Aissatou Ndong, Thierry Cutard, Ange Nzihou, Martin Piotte,
Jean-Christophe Cadot, Doan Pham Minh

► To cite this version:

Aissatou Ndong, Thierry Cutard, Ange Nzihou, Martin Piotte, Jean-Christophe Cadot, et al.. Dynamic characterization approach for the investigation of microstructural changes in clay-based materials during firing. *Open Ceramics*, 2023, 13, pp.100326. 10.1016/j.oceram.2022.100326 . hal-03918326

HAL Id: hal-03918326

<https://imt-mines-albi.hal.science/hal-03918326v1>

Submitted on 2 Jan 2023

HAL is a multi-disciplinary open access archive for the deposit and dissemination of scientific research documents, whether they are published or not. The documents may come from teaching and research institutions in France or abroad, or from public or private research centers.

L'archive ouverte pluridisciplinaire **HAL**, est destinée au dépôt et à la diffusion de documents scientifiques de niveau recherche, publiés ou non, émanant des établissements d'enseignement et de recherche français ou étrangers, des laboratoires publics ou privés.



Distributed under a Creative Commons Attribution 4.0 International License



Dynamic characterization approach for the investigation of microstructural changes in clay-based materials during firing

Aissatou Ndong^{a,b,**}, Thierry Cutard^b, Ange Nzihou^a, Martin Piotte^c, Jean-Christophe Cadot^c, Doan Pham Minh^{a,*}

^a Centre RAPSODEE, Université de Toulouse, CNRS UMR 5302, IMT Mines Albi, Campus Jarlard, F-81013 Albi, France

^b Institut Clément Ader (ICA), Université de Toulouse, CNRS UMR 5312, IMT Mines Albi, INSA, ISAE-SUPAERO, UPS, Campus Jarlard, F-81013, Albi, France

^c TERREAL, CRED, 415 Route de Revel, F-11400, Castelnaudary, France

ARTICLE INFO

Keywords:

Clay-based mixtures
Microstructural evolution
Mechanism understanding

ABSTRACT

This work aims to understand the mechanisms occurring during the microstructural transformation of clay-based mixtures. For that, the combination of various standard and advanced characterization techniques was used. This original approach allowed an outstanding description of complex mechanisms involved during the firing, bringing new insights in regards to the state-of-the-art. Thus, the formation of viscous glassy phases and the associated effects in terms of densification acceleration were particularly revealed by following the damping of Acoustic Resonance (AR) signals and by dynamic high-temperature Scanning Electron Microscopy (SEM). Further STEM-EDX (Scanning Transmission Electron Microscopy Coupled with Energy Dispersive X-ray) analyses revealed that the glassy phase resulting from the solidification of the viscous phase is predominantly composed of silicon, aluminum, oxygen, and potassium. This study also evidenced that the behavior of a binary clay-based mixture was not always described by a mixing law model.

1. Introduction

Fired clay-based mixtures are among the most used construction materials. During the firing step, important physicochemical transformation takes place in such materials. They depend on several parameters including the nature of starting materials, drying conditions, heating and cooling rates, maximum firing temperature, and the presence or not of additives [1–6]. Because of the complexity of natural clay mixtures, these transformations are not yet thoroughly evidenced. This makes the optimization of fired-clay ceramics production difficult. However, the development of new methodologies plays an important role for this industrial sector, e.g. the optimization of energetic consumption [7–10]. Up-to-date, mineralogical evolution is usually studied by X-ray diffraction (XRD) [11–14]. Miras et al. [14], for instance, showed that dynamic XRD at high-temperature allowed obtaining more precise information on the mineralogical evolutions than classical XRD at room temperature. Nevertheless, XRD techniques cannot be used to characterize either amorphous phases or crystalline phases of low contents (typically <1 wt%). To support XRD techniques, thermal analyses

such as thermogravimetric analysis (TGA), differential thermal analysis (DTA), and thermomechanical analysis (TMA) are also used [15,16]. Pontikes et al. [15], for instance, studied the thermal behavior of clay and bauxite residues (BR) mixtures, using TGA-DTA, TMA, and XRD. They revealed the formation of a viscous glassy phase that lower the sintering temperature due to the presence of boron oxide. Hernández et al. [10] reported similar results on their study using different boron sources. However, no information could be evidenced by these methods about the interaction between clay matrix and BR or boron sources.

Despite numerous mechanistic studies on the evolutions of clay-based materials, most of them were conducted on fired products at room temperature. So, less information has been published on firing. This has limited the understanding of what happens inside materials during the firing cycle. To further understand the thermal behavior of clay-based mixtures, a combination of different physicochemical and thermo-mechanical characterization techniques, under dynamic conditions, seems to be well appropriate. The objective of this study is to address this challenge, by coupling appropriate dynamic physicochemical and thermo-mechanical characterization techniques to follow

* Corresponding author. Centre RAPSODEE, Université de Toulouse, CNRS UMR 5302, IMT Mines Albi, Campus Jarlard, F-81013 Albi, France

** Corresponding author. Centre RAPSODEE, Université de Toulouse, CNRS UMR 5302, IMT Mines Albi, Campus Jarlard, F-81013 Albi, France.

E-mail addresses: aissatou.ndong@mines-albi.fr (A. Ndong), doan.phamminh@mines-albi.fr (D. Pham Minh).

microstructure evolutions of clay-based materials as a function of temperature during a firing cycle.

2. Materials and methods

2.1. Three clay-based mixtures

Two industrial clay-based mixtures based on two natural clays, named ClayMix1 and ClayMix2, were used as reference materials in this study. Each clay was extracted as one batch in a clay quarry to ensure homogeneity and was also ground at the laboratory scale with a 1 mm rolling. A third mixture containing 80 wt% of ClayMix1 and 20 wt% of ClayMix2 was also considered and named ClayMix3. The chemical analysis of the three mixtures was performed by XRF using a PanAnalytical Epsilon 3-XL equipment. The measurements were carried out in a melted glass bead. This latter was prepared by mixing a clay-based mixture sample with lithium tetraborate ($\text{Li}_2\text{B}_4\text{O}_7$), with a weight ratio of 17/83, and heated at 930 °C under air for melting. Furthermore, the mineralogical analyses of clay-based mixtures were carried out by XRD using a Philips Panalytical X'Pert Pro MPD diffractometer, which presents a limit of detection of ca. 1 wt% for each crystalline phase, working at standard conditions (Cu $K\alpha$ radiation wavelength: 1.543 Å, tension: 45 kV, current: 40 mA, 2θ angle range: 7°–80°, step size: 0.067°, step time: 29.89 s). Mineralogical phases were identified from the JCPDS and COD databases. The particle size distribution was determined on clay mixtures using a Mastersizer 2000 laser granulometer.

2.2. Preparation of monolithic samples

Monolithic samples were prepared by adding water (19, 18 and 19 wt% for ClayMix1, ClayMix2 and ClayMix3, respectively) in each clay-based mixtures, using a laboratory kneader. Grinding in a 1 mm roll mill was then performed for homogenization. Finally, $175 \times 79 \times 13$ mm³ samples were extruded at ca. 7.5–8 bar pressure before being subjected to a drying cycle with a heating rate of 1 °C/min from room temperature to 105 °C, with 24 h isothermal dwells at 25, 45, 75, and 105 °C. At the end of the drying cycle, the samples were stored in an oven maintained at 75 °C to avoid water absorption [17]. Before characterization, samples were cut and polished to the required dimensions.

2.3. Characterization of clay-based mixtures

Thermogravimetric analysis coupled with differential thermal analysis (TGA-DTA) was performed on cylindrical monolithic samples (100–200 mg in mass) using a SETARAM Labsys 92 instrument under air. Samples were heated from 30 to 1120 °C at 5 °C/min. Gas emission from this TGA-DTA was analyzed by dynamic mass spectroscopy (using an OmniStar equipment from Pfeiffer Vacuum) which allows the qualitative analysis of CO_2 , CO, and H_2O emitted from thermal decomposition.

Thermo-mechanical analysis (TMA) was carried out using a SETARAM Setsys 16/18 apparatus on cylindrical monolithic samples (diameter 5 mm, length 13 mm) under air, up to 1120 °C, at the heating rate of 5 °C/min and a cooling rate of 3 °C/min. TMA signal was monitored along the thermal cycle.

Mechanical properties were measured on $60 \times 30 \times 5$ mm³ monolithic samples using an IMCE HT650 resonant frequency analyzer in flexural mode to obtain Young's modulus (from fundamental resonance frequency and sample dimensions) and the damping of the acoustic signal (from dissipative energy), according to the ASTM-E1876-01 standard [18]. The tests were continuously performed during thermal cycles up to 1050 °C under air (heating rate of 5 °C/min, an isothermal dwell time of 1 h, and cooling rate of 3 °C/min).

For each firing temperature, a rectangular monolithic sample was crushed and ground to powder for the investigation of the mineralogical transformation by XRD.

The microstructural evolutions were also investigated by scanning electron microscopy (SEM) at room temperature on the fracture surface of samples recovered from the bending test using a Philips XL30 ESEM FEG. In addition, dynamic observations were also performed with a monolithic sample of ClayMix3 using a hot plate in the SEM equipment. Images were recorded during firing from 30 to 880 °C with a heating rate of 10 °C/min, and an isothermal dwell time of 1 h at 880 °C. Concurrently with these observations, element mappings and local elemental analysis were performed using a JEOL JEM2010 HC (with an LaB6 filament) transmission electron microscopy (TEM) at 200 kV operating in STEM (Scanning Transmission Electron Microscopy) mode with a thin lamella of ClayMix3 treated 1 h at 1000 °C. The microscope was equipped with an energy-dispersive X-ray (EDX) detector. Sample preparation for STEM was done by Focused Ion Beam (FIB). This STEM-EDX element mapping and local elemental analysis aimed to determine the chemical analysis at nanometric scale of ultra-thin lamella, in particular of the viscous glassy phase.

3. Results and discussion

3.1. Mineralogical and chemical characterizations of the as-received clay mixtures

Both mixtures have high SiO_2 contents (67.7 wt% for ClayMix1, and 71.7 wt% for ClayMix2) and moderate Al_2O_3 contents (17.5 wt% for ClayMix1 and 21.1 wt% for ClayMix2). Both clay mixtures have relatively low contents of K_2O (3.2 wt% for ClayMix1 and 2.8 wt% for ClayMix2), of MgO (0.9 wt% for ClayMix1 and 0.2 wt% for ClayMix2) and of TiO_2 (1.2 wt% for ClayMix1 and 1.5 wt% for ClayMix2). The main difference between these two clay mixtures is the high Fe_2O_3 content in ClayMix1 (9.2 wt%). In both clay mixtures, XRD analysis shows the presence of kaolinite ($\text{Al}_2\text{Si}_2\text{O}_5(\text{OH})_4$, JCPDS number: 01-075-0938), muscovite ($\text{KAl}_3\text{Si}_3\text{O}_{10}(\text{OH})_2$, JCPDS number: 01-071-1049) and quartz (SiO_2 , JCPDS number: 01-083-0539) which confirms XRF results. Laser granulometry showed a multimodal distribution in both clay mixtures. Also, ClayMix1 presents more fine particles compared to ClayMix2. This led to more mixing water requirements for the preparation of monolithic samples from ClayMix1.

3.2. Mineralogical transformation during firing

3.2.1. Thermal behavior

According to the TGA-DTA curves presented in Fig. 1, clay-based mixtures exhibit a mass loss until 150 °C (from 0.9 to 1.4 wt%), associated with an endothermic reaction ascribed to the dehydration as reported in Refs. [12,19–22]. The firing leads to a second mass loss from

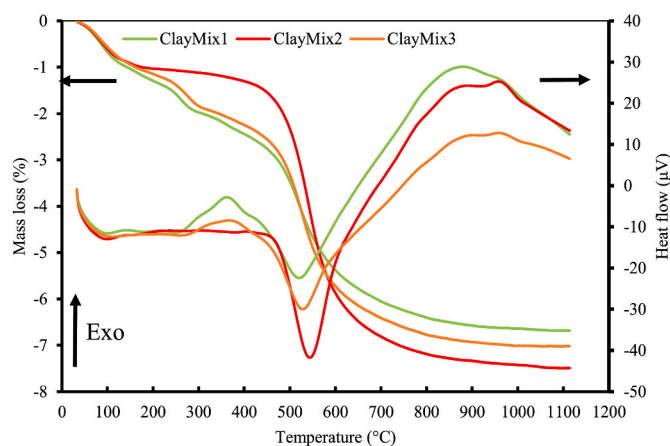


Fig. 1. Mass loss (TG) and heat flow (DTA) of ClayMix1, ClayMix2, and ClayMix3 recorded during the first heating.

150 °C to 450 °C along with an exothermic reaction for ClayMix1 and ClayMix3 by a release of CO₂ which could be attributed to the removal of organic substances, according to the work in Refs. [21–23]. Indeed, CO₂ and H₂O were identified by TGA – MS as residual gases during the firing of ClayMix1 and ClayMix3, whereas no exothermic reaction was observed for ClayMix2. Consequently, in addition to the high iron oxide Fe₂O₃ content, the presence of organic matter supported by an exothermic effect (at 350 °C), is the second parameter that distinguishes the ClayMix1 and ClayMix2. The second endothermic peak, recorded during the firing, is a large peak centered at 550 °C which could be partially attributed to the decomposition of the hydroxyls groups (OH) of kaolinite and muscovite. This dehydroxylation was overlapped with the change in the crystal structure of the quartz [19,20,24–26]. The mass loss of this dehydroxylation (reach wt. = 3, 5, and 3.5 wt% for ClayMix1, ClayMix2, and ClayMix3) is more important for ClayMix2 than ClayMix1 and ClayMix3. Furthermore, the reactions and temperatures at which they occur will be clearly identified in sections 3.2.2 and 3.2.4. Dynamic MS analysis of gas from the outlet of TGA-DTA allowed detecting the release of CO₂ in the 650–850 °C range. This could be attributed to the decarbonation of carbonate salts such as CaCO₃. The total mass loss recorded during the firing was 6.7 wt%, 7.5 wt%, and 7 wt% for ClayMix1, ClayMix2, and ClayMix3 respectively.

TGA-DTA results (Fig. 1) also reveal exothermic peaks of low intensity above 800 °C that could be related to the sintering phenomenon [8,22,25,27,28]. This could be due to solid-state chemical reactions or to the formation of a liquid phase previously observed with a hot stage transmission electron microscope by McConville and Lee [24,29].

3.2.2. Thermomechanical behavior

The results of the TMA of the three mixtures are shown in Fig. 2. Up to 150 °C, a low shrinkage is observed and can be related to the mass loss

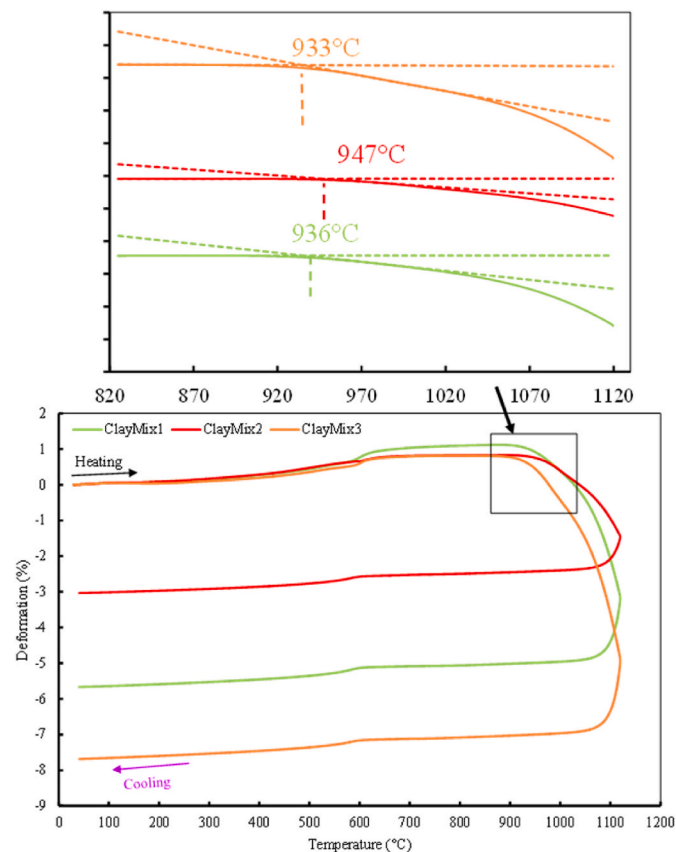


Fig. 2. – Deformation (TMA) of ClayMix1, ClayMix2, and ClayMix3 during firing.

induced by dehydration. Then, the materials have a slow expansion up to 900 °C. The expansion phenomena recorded close to 600 °C can be assigned to $\alpha \rightarrow \beta$ quartz transition. Above 900 °C, the three clay mixtures exhibit a pronounced shrinkage, from approximately 936 °C, 947 °C, and 933 °C for ClayMix1, ClayMix2, and ClayMix3 respectively, up to the maximum temperature of the cycle (1120 °C). Shrinkage is already measured during the beginning of the cooling. Then the behavior moves to a more classical linear one, due to thermal contraction of the materials. A dilatometric phenomenon is observed close to 600 °C and can again be attributed to the allotropic transformation of quartz. The final shrinkage is of 6.8%, 3.8%, and 8.4% for ClayMix1, ClayMix2, and ClayMix3 respectively. TGA-DTA analysis (Fig. 1) revealed exothermic reactions above 800 °C for all three mixtures, which could be caused by accelerated densification as reported by McConville and Lee [24] and Nigay et al. [22]. In particular, ClayMix1 started the densification earlier than ClayMix2. This could be explained by the fact that finer particles sinter faster and more glassy phase forms providing better sintering according to the previous studies in Refs. [15, 30] and its high fluxing oxides content such as Fe₂O₃ and K₂O [31,32]. This behavior is in agreement with its high shrinkage compared to ClayMix2. Besides, the highest shrinkage is observed for ClayMix3. This could be attributed to a significant interaction between ClayMix1 and ClayMix2, which led to accelerated densification.

3.2.3. Mineralogical transformation

The mineralogical transformation (Fig. 3) of the three clay-based mixtures was studied by X-ray diffraction after firing at different temperatures in the 800–1120 °C range.

Referring to the results of TGA-DTA analysis and TMA, firing at 800 °C induced the decomposition of kaolinite and muscovite (dehydroxylation), which is manifested by the presence in XRD patterns of anhydrous illite peaks (JCPDS number: 00-046-0741). Quartz (JCPDS number: 01-083-0539) and hematite (JCPDS number: 01-086-0550) were not affected by the firing. However, peaks of metakaolinite were not identified in the diffractograms as a result of the destruction of its crystalline structure.

Nonetheless, albite (NaAlSi₃O₈, JCPDS number: 00-001-0739) was detected in ClayMix1. Consequently, further evidence of the presence of anhydrous illite could be provided by SEM observations at ambient temperature after firing at 800 °C and 900 °C, a phase characterized by its layered microstructure (Fig. 4).

Also, XRD results suggest that hematite develops between 800 and 900 °C in all mixtures and remain present at 1120 °C. It is worth noting from these results that iron is originally present in all clay mixtures, although it was not detected in XRD patterns of the raw materials. According to Ref. [24] iron is present in clay mixture as either a substitutional impurity or an amorphous oxyhydroxide surface layer. This could explain the reasons why peaks of crystalline phases containing iron were not identified in XRD.

By increasing the firing temperature, anhydrous illite peak intensity decreases gradually. Besides, quartz is detected after all firing temperatures (up to 1120 °C). However, its peak intensity starts to decrease when the firing temperature reaches 1000 °C, suggesting its partial dissolution into the viscous glassy phase formed in the clay-based mixture. Somehow, the presence of iron oxide and alkaline oxide promoted densification by a formation of a viscous glassy phase, which makes the penetration of this phase into the pores easier [21,33,34]. In Ref. [35], the authors indicated that the dissolution should be accompanied by an increase in the viscous glassy phase content [36].

However, previous studies by Khalfaoui et al. [33] and Ranogajec et al. [1] showed that the illite breakdown products presumably constituted a framework for the viscous glassy phase, and the liquid K-enrichment led to the formation of Al–Si–O complexes which should increase the melt viscosity. In his work, McConville and Lee [24] went further by affirming that the tetrahedral part of the relict illite structure combines with any alkalis present to form the viscous glassy phase,

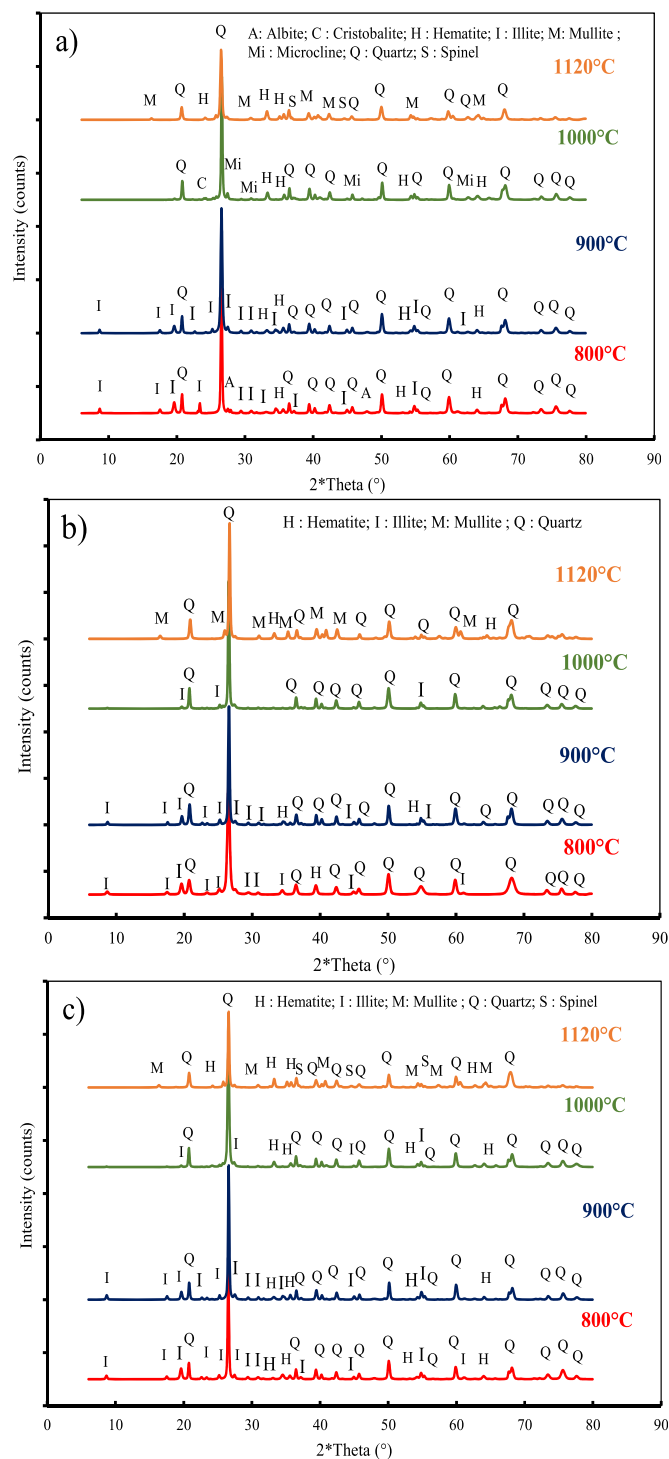


Fig. 3. X-rays diffractograms of ClayMix1 (a), ClayMix2 (b), and ClayMix3 (c) after firing at 800 °C, 900 °C, 1000 °C, and 1120 °C.

beginning at 950 °C. This later theory could explain the abrupt shrinkage, above 900 °C observed in TMA results, related to the acceleration of densification.

Firing at 1000 °C leads to the formation of microcline (KAlSi₃O₈, JCPDS number: 00-001-0705) and of cristobalite (JCPDS number: 01-082-1407) in ClayMix1, whereas quartz and anhydrous illite were only identified in ClayMix2 for this temperature.

In view of the above results, the investigation of the mineralogical transformation during the firing of clay-based mixtures through conventional techniques such as TGA-DTA, TMA, and XRD shows that the

three clay mixtures present many similarities in their behavior. Thus, the mechanisms by which the transformation takes place appear to be similar. Overall, after dehydroxylation of the three clay mixtures, the original crystal structure observed by XRD is lost for kaolinite, while in the case of illite it is maintained till 900 °C. The sintering led to a densification in the presence of a viscous glassy phase, which induced the development of dense microstructure (Fig. 4). After firing at 1120 °C, an Al/Mg spinel phase (Mg₈Al₁₆O₃₂, JCPDS number: 96-900-2131), mullite (Si₂Al₆O₁₃, JCPDS number: 00-001-0613), and quartz for ClayMix1 and ClayMix3 were identified (Fig. 3) by XRD. However, these techniques do not give enough information on what happens during the sintering step. As a consequence, two original approaches for clay-based ceramics have been carried out to obtain specific data on sintering mechanisms by following the damping of acoustic resonance signals and by dynamic high-temperature SEM observations.

3.2.4. Damping of acoustic resonance signals and dynamic high-temperature SEM observations during a first heating

Evolutions of damping of the acoustic resonance signals for the three clay-based mixtures during the first heating are shown in Fig. 5. From room temperature up to 200 °C, the results show a decrease of damping due to the evaporation of the residual free water, in agreement with the results considered in sections 3.2.1 and 3.2.2. At higher temperatures, when the bondings are broken during dehydroxylation of clay minerals, an increase of damping is observed. This is mainly observed from 450 °C and most particularly in ClayMix2. It must be observed that the amplitude of the damping dome for the ClayMix2 mixture is the highest one as the mass loss and the heat flow decrease were the highest ones for this same mixture and these same dehydroxylation phenomena. Subsequently, the expulsion of the hydroxyl groups caused a progressive reduction in the damping of the acoustic signal, whereas a slight increase is observed above 600 °C, related to the consequence of the transformation of quartz at 573 °C [37].

At higher temperatures, an increase in the damping of the acoustic signal starts at 910 °C for ClayMix1 and ClayMix2, and 880 °C for ClayMix3. This is characteristic of a flow region in the material behavior [38,39]. Between the three mixtures, the same order is conserved than the one observed by considering the temperature levels for the beginning of densification on TMA curves. But the temperature levels are lower for damping compared to shrinkage. The difference varies from 26 °C for ClayMix1 to 53 °C for ClayMix3. This must be related to the high sensitivity of damping to the formation of viscous phases or flows in a material. TMA and damping results are fully complementary ones and are in agreement with previous results indicating the formation of viscous and liquid glassy phases in clay-based materials [40]. As mentioned above, the formation of the liquid phase is attributed to the presence of alkali oxides, as well as iron oxide [21,41]. However, the alkalis are derived from the muscovite present in raw materials and induce a melting at a lower temperature level [2,42–44]. Moreover, the viscosity of the liquid phase decreases with the temperature rising.

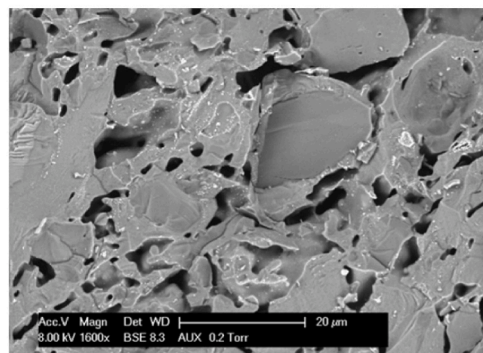
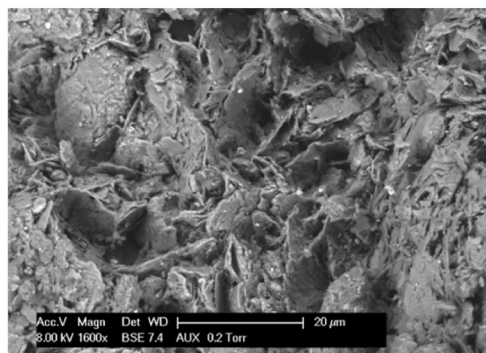
Referring to the results reported in Ref. [33], the magnesium involved in the crystallization of the Al/Mg spinel phase, identified in XRD results (section 3.2.3), should be derived either from illite or chlorite, which is in agreement with the considered clays partially composed by illite. This is consistent with the theory that potassium supplied by illite is mainly involved in the low viscosity liquid phase formation that accelerates sintering [31,45]. However, it has been reported that high iron oxide content can promote the earlier appearance of liquid with low viscosity.

Formation of viscous glassy phase was confirmed by SEM observations after firing at 1000 °C in each clay-based mixture. As examples, SEM pictures (Fig. 6) observed after firing at 1000 °C for ClayMix3. Overall, SEM micrographs reveal a visible change in morphology, among other, thicker layer (due to the binding of layers between them by diffusion) with spacing between layers, contraction (due to the densification), and the apparition of new phases. Furthermore, the

ClayMix1

900°C

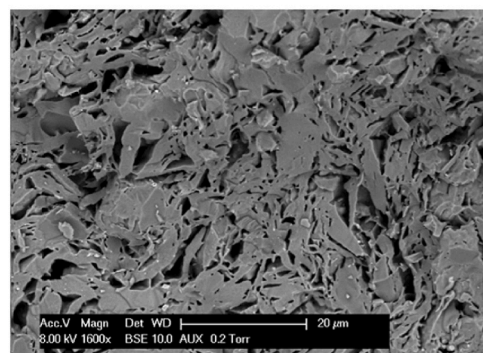
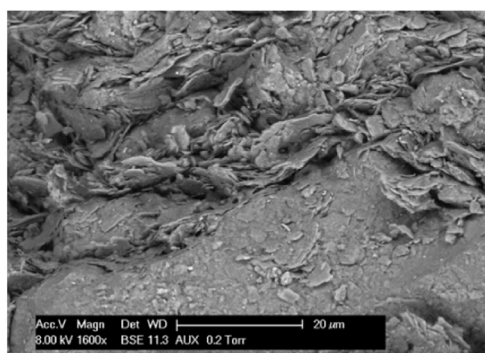
1120°C



ClayMix2

900°C

1120°C



ClayMix3

900°C

1120°C

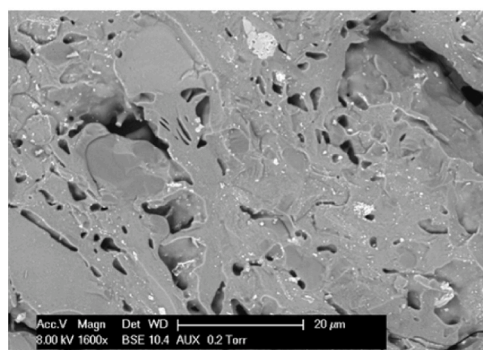
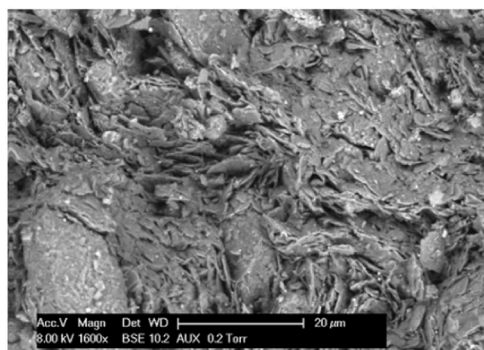


Fig. 4. SEM micrographs of ClayMix1, ClayMix2, and ClayMix3 after firing at 900 °C and 1120 °C.

interconnectivity among layers is ensured by the viscous glassy phase acting as a bridge.

Dynamic SEM observations have been performed using a hot stage, during an isothermal dwell of 1 h at 880 °C. Attention has been paid to a clay-rich area and the formation of liquid and/or viscous phases. In Fig. 7, micrographs show the progressive formation and flow of a viscous glassy phase in the ClayMix3 mixture. After 30 min, the multi-layered clay microstructure remains visible and the first evidence of liquid formation is seen, mainly close to the clay layers. When time at 880 °C increases, an increase of the amount of viscous glassy phase is clearly observed as well as its flow by capillarity phenomena. Such results are in good agreement with damping results in terms of viscous glassy phase

formation at such temperature levels. Moreover, this method gave access to the dynamic of viscous glassy phase formation at microscopic scale and mechanisms that come after this formation such as pore filling by the viscous flow (by capillarity effect) and the increase of the amount of this phase which leads to the acceleration of the densification. Using dynamic SEM observation in clay mixture gave more precise information than conventional methods as long as that confirms phenomena that were previously only hypothesized like densification acceleration attributed to viscous glassy phase formation.

In parallel, a composition mapping of the elements present in the microstructure of the ClayMix3 sample which was thermally treated at 1000 °C was investigated by STEM-EDX measurements. The STEM-EDX

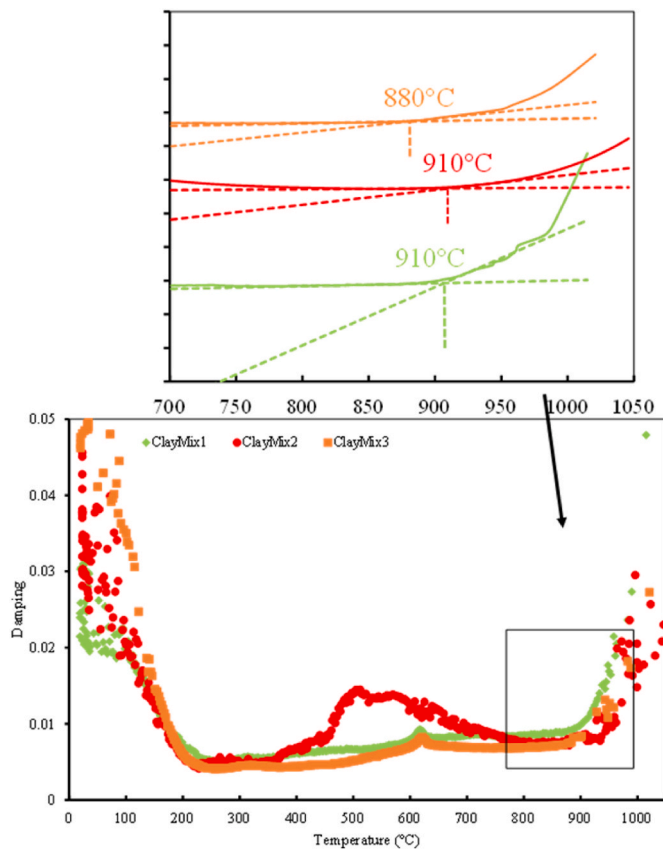


Fig. 5. Damping of ClayMix1, ClayMix2, and ClayMix3 during heating.

mapping, shown in Fig. 8, reveal that the microstructure of the analyzed sample is consisted mainly of two different areas (Fig. 8(a)), a clay matrix area and the glassy phase one. It has been observed the presence of the glassy phase inside the porosity, in some cases, due to the viscous glassy phase penetration.

The clay matrix area is characterized by an enrichment in Al (Fig. 8(c)), Si (Fig. 8(e)) and O (Fig. 8(d)), whereas as the glassy phase is enriched in K (Fig. 8(b)) and additionally Si, Al and O were detected. This result suggests that the K from the anhydrous illite appears to play a major role in the formation of the viscous glassy phase. Many studies emphasizes the importance of the alkaline and iron oxide in the viscous glassy phase formation, however Fe was not detected in the glassy phase area from the elemental mapping.

A semi-quantitative elemental evaluation provided by EDX in a selected local area in the clay matrix area (Fig. 9(a)) showed a high content (atomic proportion ≥ 10 %at) of O, Si and Al, a lower content (atomic proportion ≤ 1 %at) of Fe, K, and Mg. This local analysis showed the presence of the elements constituting anhydrous illite and quartz identified by EDX. In addition, the relative proportions between elements (Si, Al, O and K) correlate with these two crystalline phases identified for the clay matrix. On the hand, a strong presence (atomic proportion ≥ 10 %at) of O and Si, a moderate content (atomic proportion: 2–9 %at) of Al and K, and a small content (atomic proportion ≤ 1 %at) of Fe and Mg were detected in the glassy phase area (Fig. 9(b)). This result showed that the viscous glassy phase is mainly composed of oxygen, silicon, aluminum and potassium. There appears an increase of the potassium content in this area, thus confirming the enrichment of the viscous phase in K and the preponderant role of potassium in the formation of the viscous glassy phase formation and on the densification. Furthermore, the contribution of Mg and Fe in the formation of the viscous glassy phase is not significant. This result is consistent with the one from the elemental mapping.

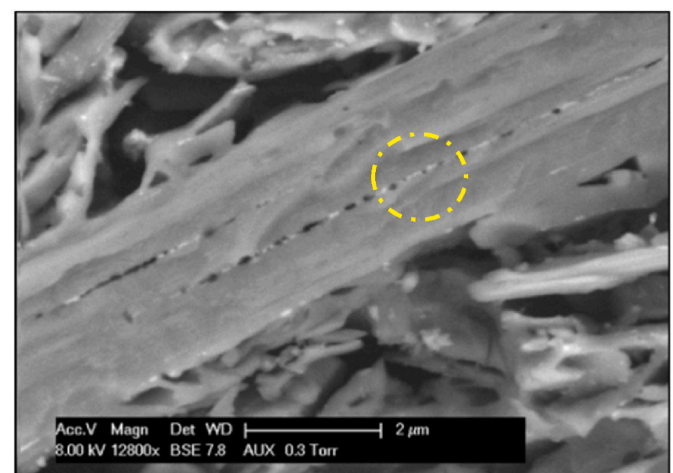
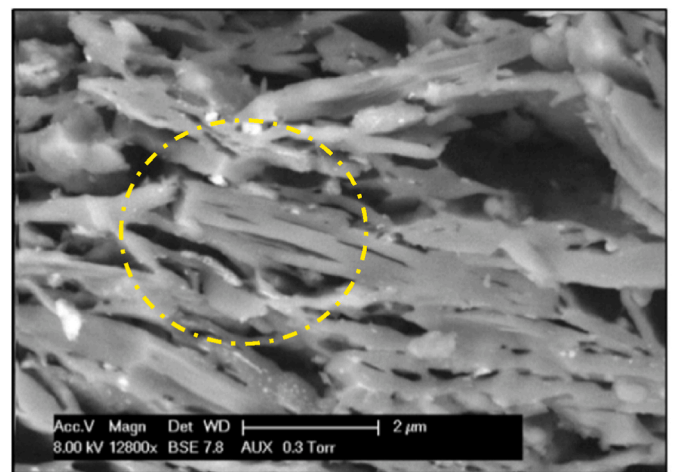
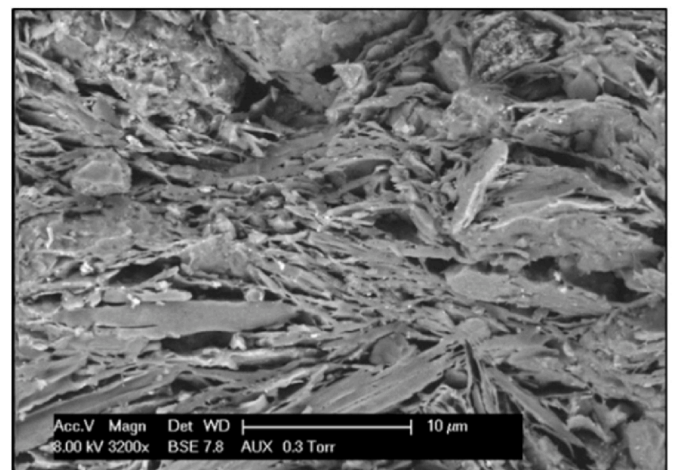


Fig. 6. Room temperature SEM micrographs of ClayMix3 after firing at 1000 °C.

3.2.5. Elastic properties during firing

Evolutions of the Young modulus of ClayMix1, ClayMix2, and ClayMix3 during firing are shown in Fig. 10. After drying at 30 °C, the three mixtures are characterized by the Young modulus of 5 GPa, 6 GPa, and 7 GPa, respectively. No significant deviation was observed.

The evaporation of the residual free water up to 150 °C leads to Young's modulus increases of 19.6%, 29.2%, and 19.7% for ClayMix1, ClayMix2, and ClayMix3. The dehydroxylation of clay-based minerals, overlapped with the crystal change of the quartz from 450 °C to 600 °C, does not bring out to a significant change in Young modulus. However, a

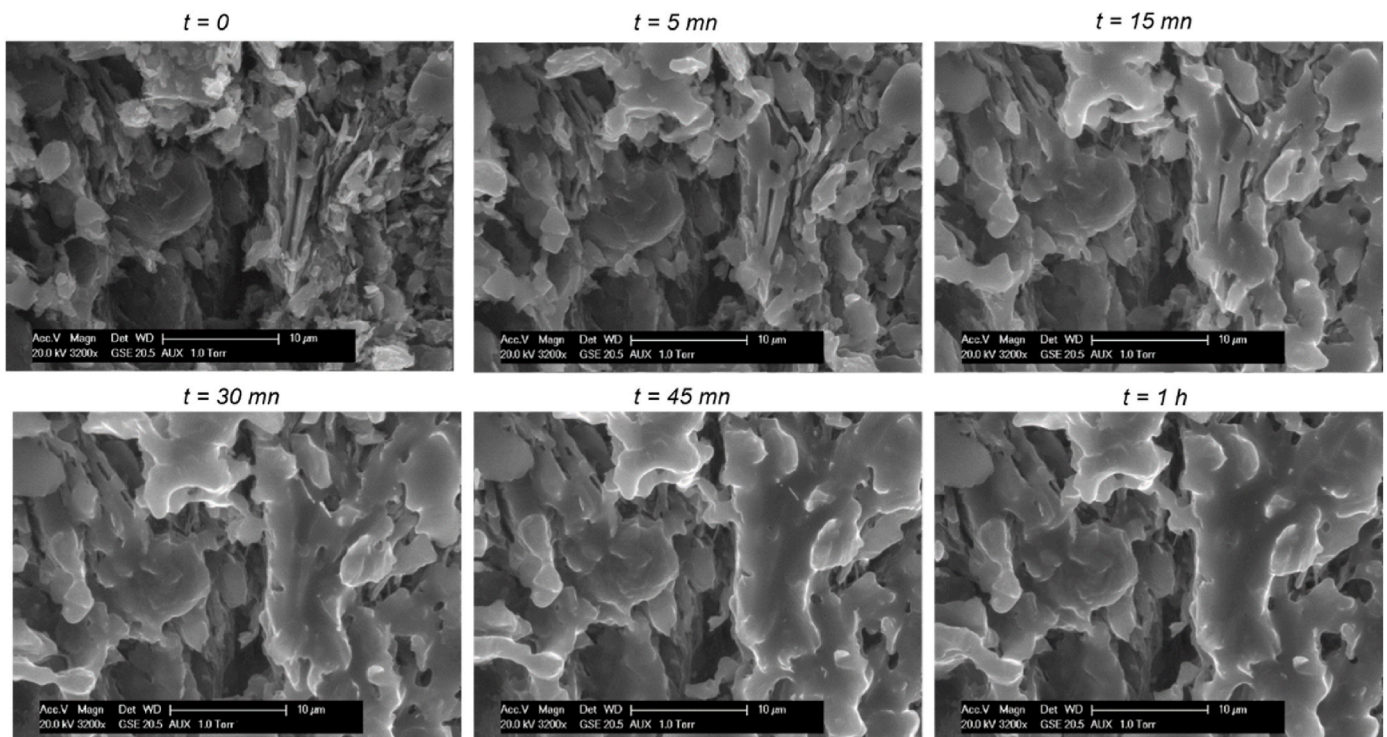


Fig. 7. High temperature dynamic SEM micrographs of ClayMix3, during the first heating (isothermal dwell of 1 h at 880 °C).

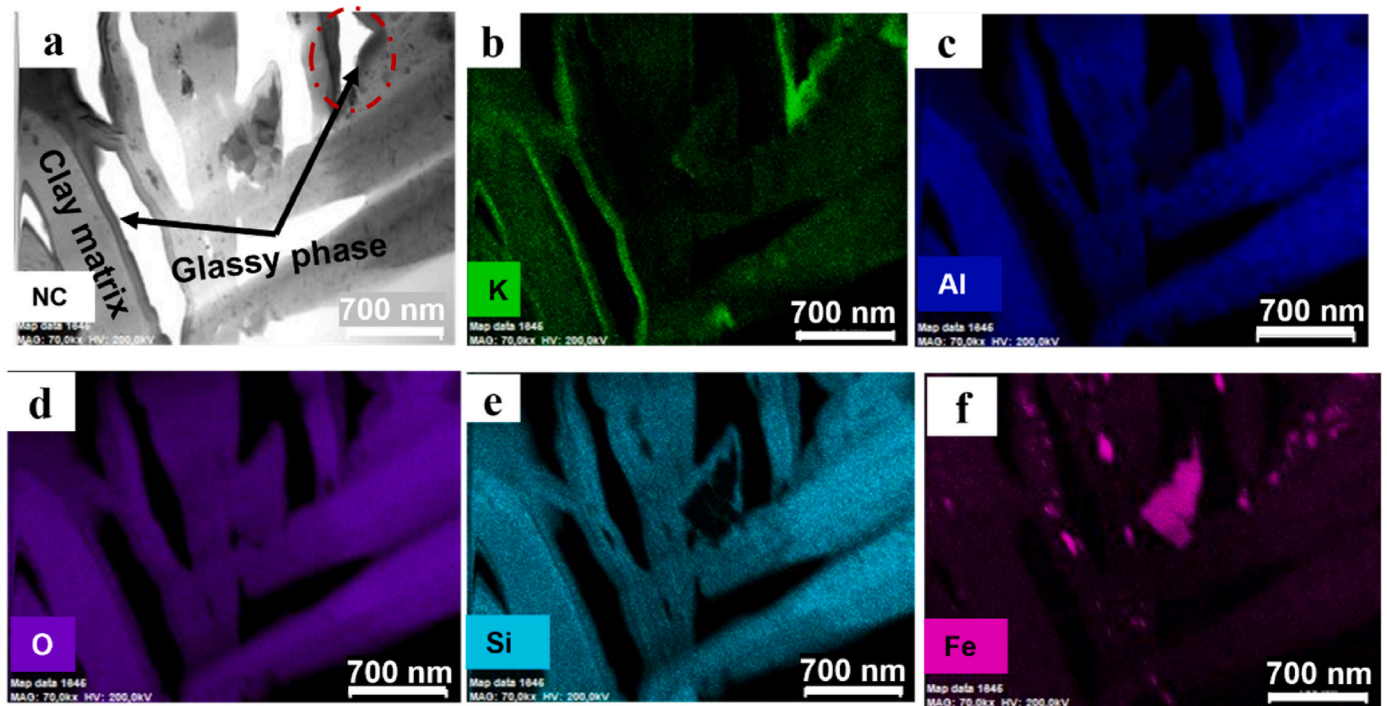


Fig. 8. STEM-EDX elemental mapping of ClayMix3 after firing at 1000 °C. The arrows indicate the glassy phase and the dotted circle presents an illustration of the wetting of the clay matrix by the viscous glassy and the closing of the porosity by capillary effects.

slight decrease is observed during $\alpha \rightarrow \beta$ quartz inversion for all mixtures. Decarbonation, identified by TGA-MS, does not significantly change Young's modulus too. Then Young modulus starts to increase at 915 °C, 930 °C and 925 °C for ClayMix1, ClayMix2, and ClayMix3 up to 1050 °C, the maximum temperature of the thermal cycle for acoustic resonance measurements. This increase is induced by the densification

and the crystallization of the metakaolin to an Al/Si spinel phase, which is not detected in XRD, in this study, based on the work in Refs. [22,40]. Young modulus is more important for ClayMix3 at the end of the isothermal dwell at 1050 °C; this is explained by the earliest formation of the viscous glassy phase in this clay mixture inducing the densification, which is consistent with the shrinkage. According to the study by

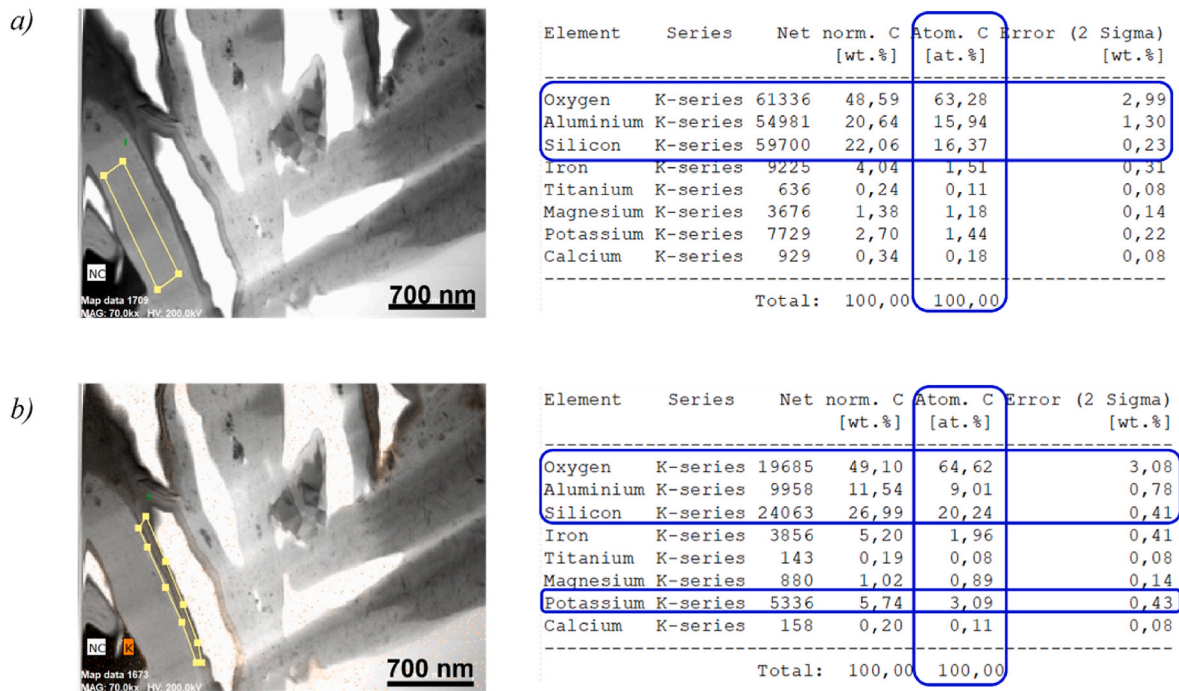


Fig. 9. Semi-quantitative elemental evaluation provided by STEM-EDX in a selected local area of ClayMix3 sample.

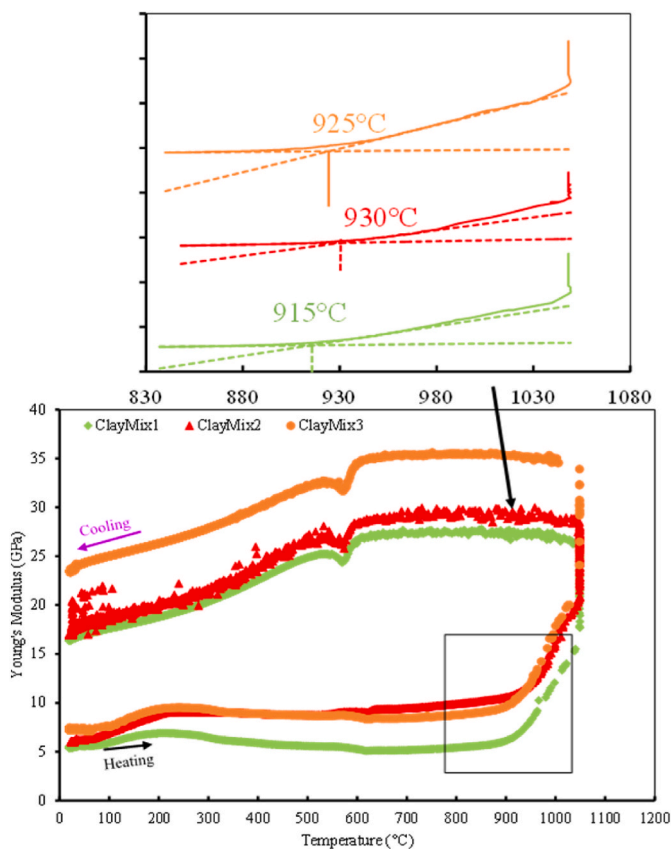


Fig. 10. Young's modulus of ClayMix1, ClayMix2, and ClayMix3 during firing.

Pialy et al. (2009) on the effects of the densification on the evolution of the elastic properties of clay-based material during firing, the evolution of Young modulus (above 800 °C) should occur simultaneously with a decrease in porosity due to the development of viscous and liquid glassy

phases.

Nevertheless, the first part of the cooling step (in the 1050 to 850 °C temperature range) is marked by a low and continuous increase of Young modulus due to the creation of glassy phases resulting from the solidification of the viscous glassy phase and the viscous flow. Then the Young modulus is quite constant in the 850 to 600 °C temperature range. From 600 °C to 30 °C, Young modulus decreases significantly for all the clay-based materials by 47% up to 63%. This behavior is associated with the crystal change $\beta \rightarrow \alpha$ quartz inversion at 573 °C, causing a diffuse microcracking mainly by debonding at clay matrix/quartz interfaces (example in Fig. 11). Moreover, no liquid was observed on the interfaces of clay matrix-quartz and clay matrix-agglomerate at this temperature. Hence, ClayMix1, ClayMix2, and ClayMix3 showed Young's modulus of 16 GPa, 17 GPa, and 23 GPa respectively after cooling. However, ClayMix3 showed the highest Young modulus after the first firing cycle, which indicates that all the properties and mechanisms of this clay-based mixture could not be explained by a mixing law model.

4. Conclusions and perspectives

This work was focused on the investigation of the thermal behavior of clay-based mixtures using a combination of dynamic characterization techniques. Results revealed that combining dynamic characterization techniques has been suitable to identify and depict mechanisms occurring during firing compared to conventional techniques such as XDR and TGA-DTA. Accordingly, particular attention has been focused on the high-temperature range (800–1120 °C). For the first time, the use of the damping signal in clay-based mixtures revealed the formation of viscous and liquid glassy phases, which led to the acceleration of densification. This has been identified using dynamic observations in hot plate on SEM. However, the results revealed that the presence of potassium in raw materials, mainly derived from muscovite/illite, induced viscous glassy phase formation at a lower temperature, which led to the acceleration of the densification. The STEM-EDX measurements of the Clay-Mix3 sample confirmed the assumption that the presence of potassium in the raw material promote the densification by a formation of a viscous glassy phase, which was mainly composed by oxygen, silicon, aluminum and potassium. Furthermore, the results also revealed that the behavior

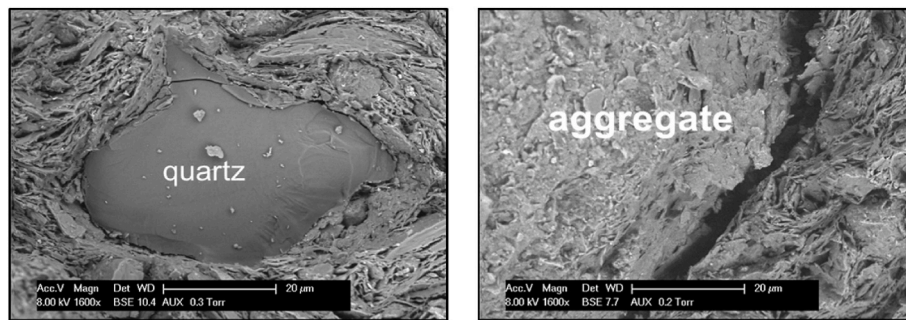


Fig. 11. Room temperature SEM micrographs of clay matrix-quartz interfaces and of clay matrix-aggregate interfaces for ClayMix3 after firing at 1000 °C.

of a binary mixture containing different clay-based mixtures could not always be described with a mixing law model. In fact, such a model could be used to describe decomposition mechanisms, while other mechanisms depend on the chemical and mineralogical composition, as well as on the physical properties of the raw materials.

The results of this study suggest that a combination of physico-chemical and thermo-mechanical analyses using characterization techniques under dynamic conditions is essential to accurately identify and describe the mechanisms and the temperature at which the phase developments take place during the firing of clay-based materials. This original approach can be used to predict the desired final microstructure and promote a decrease in the firing temperature of clay-based materials in which various additives could have been added.

Declaration of competing interest

The authors declare that they have no known competing financial interests or personal relationships that could have appeared to influence the work reported in this paper.

Acknowledgments

The authors gratefully acknowledge the financial, scientific, and technical supports from TERREAL Company (CRED) to this research. The support from l'Agence Nationale de la Recherche (ANR) under the LabCom RESPECTc project is also acknowledged. We also would like to thank the staff at CEMES-CNRS, and ICA and RAPSODEE Center (IMT Mines Albi) for technical assistance in this research.

References

- [1] J. Ranogajec, M. Djuric, M. Radeka, P. Jovanic, Influence of particle size and furnace atmosphere on the sintering of powder for tiles production, *Ceram-Silik* 44 (2000) 71–77.
- [2] G. Cultrone, E. Sebastián, K. Elert, M.J. de la Torre, O. Cazalla, C. Rodríguez-Navarro, Influence of mineralogy and firing temperature on the porosity of bricks, *J. Eur. Ceram. Soc.* 24 (2004) 547–564, [https://doi.org/10.1016/S0955-2219\(03\)00249-8](https://doi.org/10.1016/S0955-2219(03)00249-8).
- [3] E. Grim Ralph, Relation of the composition to the properties of clays, *J. Am. Ceram. Soc.* 22 (2006) 141–151.
- [4] S. Freyburg, A. Schwarz, Influence of the clay type on the pore structure of structural ceramics, *J. Eur. Ceram. Soc.* 27 (2007) 1727–1733, <https://doi.org/10.1016/j.jeurceramsoc.2006.04.158>.
- [5] V.G. Lee, T.H. Yeh, Sintering effects on the development of mechanical properties of fired clay ceramics, *Mater. Sci. Eng.* 485 (2008) 5–13, <https://doi.org/10.1016/j.msea.2007.07.068>.
- [6] C. Bories, M.E. Borredon, E. Vedrenne, G. Vilarem, Development of eco-friendly porous fired clay bricks using pore-forming agents: a review, *J. Environ. Manag.* 143 (2014) 186–196, <https://doi.org/10.1016/j.jenvman.2014.05.006>.
- [7] A. Zimmer, C.P. Bergmann, Fly ash of mineral coal as ceramic tiles raw material, *Waste Manag.* 27 (2007) 59–68, <https://doi.org/10.1016/j.wasman.2006.01.009>.
- [8] A. Christogerou, T. Kavas, Y. Pontikes, S. Koyas, Y. Tabak, G.N. Angelopoulos, Use of boron wastes in the production of heavy clay ceramics, *Ceram. Int.* 35 (2009) 447–452, <https://doi.org/10.1016/j.ceramint.2007.12.001>.
- [9] Z. Zhang, Y.C. Wong, A. Arulrajah, S. Horpibulsuk, A review of studies on bricks using alternative materials and approaches, *Construct. Build. Mater.* 188 (2018) 1101–1118, <https://doi.org/10.1016/j.conbuildmat.2018.08.152>.
- [10] M.F. Hernández, P.V. López, M.S. Conconi, N.M. Rendtorff, Effect of boron sources in the thermal behavior of a clay-based ceramics, *Open Ceram* 9 (2022), 100227, <https://doi.org/10.1016/j.oceram.2022.100227>.
- [11] M.P. Riccardi, B. Messiga, P. Dumínico, An approach to the dynamics of clay firing, *Appl. Clay Sci.* 15 (1999) 393–409, [https://doi.org/10.1016/S0169-1317\(99\)00032-0](https://doi.org/10.1016/S0169-1317(99)00032-0).
- [12] M.J. Trindade, M.I. Dias, J. Coroado, F. Rocha, Mineralogical transformations of calcareous rich clays with firing: a comparative study between calcite and dolomite rich clays from Algarve, Portugal, *Appl. Clay Sci.* 42 (2009) 345–355, <https://doi.org/10.1016/j.clay.2008.02.008>.
- [13] F. Pardo, S. Meseguer, M.M. Jordán, T. Sanfeliu, I. González I, Firing transformations of Chilean clays for the manufacture of ceramic tile bodies, *Appl. Clay Sci.* 51 (2011) 147–150, <https://doi.org/10.1016/j.clay.2010.11.022>.
- [14] A. Miras, E. Galán, I. González, A. Romero-Baena, D. Martín, Mineralogical evolution of ceramic clays during heating. An ex/in situ X-ray diffraction method comparison study, *Appl. Clay Sci.* 161 (2018) 176–183, <https://doi.org/10.1016/j.clay.2018.04.003>.
- [15] Y. Pontikes, P. Nikolopoulos, G.N. Angelopoulos, Thermal behaviour of clay mixtures with bauxite residue for the production of heavy-clay ceramics, *J. Eur. Ceram. Soc.* 27 (2007) 1645–1649, <https://doi.org/10.1016/j.jeurceramsoc.2006.05.067>.
- [16] L. Beddiar, F. Sahnoune, M. Heraiz, D. Redaoui, Thermal transformation of fired clay ceramics by dilatometric analysis, *Acta Phys. Pol., A* 134 (2018) 86–89, <https://doi.org/10.12693/APhysPolA.134.86>.
- [17] R.E. Grim, W.F. Bradley, Rehydration and dehydration of the clay minerals, *Am. Mineral.* 33 (1948) 50–59.
- [18] ASTM International, West ConshohockenE28 Committee, Dynamic Young's Modulus, Shear Modulus, and Poisson's Ratio by Impulse Excitation of Vibration, ASTM International, PA, 2001. ASTM E1876-01, Standard Test Method for.
- [19] M.J. Orts, A. Escardino, J.L. Amorós, F. Negre, Microstructural changes during the firing of stoneware floor tiles, *Appl. Clay Sci.* 8 (1993) 193–205.
- [20] E. Murad, U. Wagner, Clays and clay minerals: the firing process, *Hyperfine Interact.* 117 (1998) 337–356.
- [21] T. Deng, J. Li, Study on preparation of thermal storage ceramic by using clay shale, *Ceram. Int.* 42 (2016) 18128–18135, <https://doi.org/10.1016/j.ceramint.2016.08.126>.
- [22] P.M. Nigay, T. Cutard, A. Nzihou, The impact of heat treatment on the microstructure of a clay ceramic and its thermal and mechanical properties, *Ceram. Int.* 43 (2017) 1747–1754, <https://doi.org/10.1016/j.ceramint.2016.10.084>.
- [23] L. Maritan, L. Nodari, C. Mazzoli, A. Milano, U. Russo, Influence of firing conditions on ceramic products: experimental study on clay rich in organic matter, *Appl. Clay Sci.* 31 (2006) 1–15, <https://doi.org/10.1016/j.clay.2005.08.007>.
- [24] C.J. McConville, W.E. Lee, Microstructural development on firing illite and montmorillonite clays compared with that in kaolinite, *J. Am. Ceram. Soc.* 88 (2005) 2267–2276, <https://doi.org/10.1111/j.1551-2916.2005.00390.x>.
- [25] S.Y. Reyes Lopez, J.S. Rodríguez, S.S. Sueyoshi, Microstructural characterization of sanitaryware, the relationship spinel and mullite, *J. Ceram. Process. Res.* 14 (2013) 492–497.
- [26] L. Beddiar, F. Sahnoune, M. Heraiz, D. Redaoui, Phase transformation and sintering of Algeria clay powder, *Acta Phys. Pol., A* 131 (2017) 566–568, <https://doi.org/10.12693/APhysPolA.131.566>.
- [27] A.B. Bourlinois, D.D. Jiang, P.E. Giannelis, Clay–Organosiloxane hybrids: a route to cross-linked clay particles and clay monoliths, *Chem. Mater.* 16 (12) (2004) 2404–2410, <https://doi.org/10.1021/cm049975z>.
- [28] F. Cambier, I. N'dala, M. Deletter, M.R. Anseau, Analysis of the influence of additives on the sintering of kaolinite based ceramics, *Silic. Ind.* 49 (1984) 219–225.
- [29] T. Húlan, I. Štubňa, Young's modulus of kaolinite-illite mixtures during firing, *Appl. Clay Sci.* 190 (2020), 105584, <https://doi.org/10.1016/j.clay.2020.105584>.
- [30] V.A. Leshina, A.L. Pivnev, Ceramic wall materials using glass waste, *Glass Ceram.* 59 (2002) 356–358, <https://doi.org/10.1023/A:1022090814669>.
- [31] S. Salem, A. Salem, Shrinkage prediction during non-isothermal sintering in the presence liquid phase: new kinetic model, Part I, *Thermochim. Acta* 575 (2014) 322–330, <https://doi.org/10.1016/j.tca.2013.11.004>.
- [32] M.U. Rehman, M. Ahmad, K. Rashid, Influence of fluxing oxides from waste on the production and physico-mechanical properties of fired clay brick: a review, *J. Build. Eng.* 27 (2020), 100965, <https://doi.org/10.1016/j.jobte.2019.100965>.

- [33] A. Khalfaoui, S. Kacim, M. Hajjaji, Sintering mechanism and ceramic phases of an illitic-chloritic raw clay, *J. Eur. Ceram. Soc.* 26 (2006) 161–167, <https://doi.org/10.1016/j.jeurceramsoc.2004.10.030>.
- [34] N. Nawaukaratharnant, A. Thueploy, S. Khunthon, S. Nilpairach, A. Theerapapvisetpong, Improving the technological properties of red stoneware tiles derived from Ratchaburi red clay by the addition of iron oxide, *Case Stud. Constr. Mater.* 16 (2022), e00983, <https://doi.org/10.1016/j.cscm.2022.e00983>.
- [35] J. Martín-Márquez, A.G. de la Torre, M.A.G. Aranda, J.M. Rincón, M. Romero, Evolution with temperature of crystalline and amorphous phases in porcelain stoneware, *J. Am. Ceram. Soc.* 92 (2009) 229–234, <https://doi.org/10.1111/j.1551-2916.2008.02862.x>.
- [36] S. Reyes Lopez, J.S. Rodríguez, S. Satoshi, Determination of the activation energy for densification of porcelain stoneware, *J. Ceram. Process. Res.* 12 (3) (2011) 228–232.
- [37] A.K. Chakraborty, *Phase Transformation of Kaolinite Clay*, Springer India, New Delhi, 2014, <https://doi.org/10.1007/978-81-322-1154-9>.
- [38] M. Lalanne, Review: modeling damping in mechanical engineering structures, *Shock Vib.* 7 (2000), 263–263.
- [39] A. Al Majid, R. Dufour, Formulation of a hysteretic restoring force model. Application to vibration isolation, *Nonlinear Dynam.* 27 (2002) 69–85, <https://doi.org/10.1023/A:1017937328860>.
- [40] P. Pialy, N. Tessier-Doyen, D. Njopwouo, J.P. Bonnet, Effects of densification and mullitization on the evolution of the elastic properties of a clay-based material during firing, *J. Eur. Ceram. Soc.* 29 (2009) 1579–1586, <https://doi.org/10.1016/j.jeurceramsoc.2008.09.020>.
- [41] J.J. Biernacki, A.K. Vazrala, H. Wayne Leimer, Sintering of a class F fly ash, *Fuel* 87 (2008) 782–792, <https://doi.org/10.1016/j.fuel.2007.08.024>.
- [42] C. Rodriguez-Navarro, G. Cultrone, A. Sanchez-Navas, E. Sebastian, TEM study of mullite growth after muscovite breakdown, *Am. Mineral.* 88 (2003) 713–724, <https://doi.org/10.2138/am-2003-5-601>.
- [43] G. Sedmale, I. Sperberga, U. Sedmalis, Z. Valancius, Formation of high-temperature crystalline phases in ceramic from illite clay and dolomite, *J. Eur. Ceram. Soc.* 26 (2006) 3351–3355, <https://doi.org/10.1016/j.jeurceramsoc.2005.10.012>.
- [44] G.L. Lecomte, J.P. Bonnet, P. Blanchart, A study of the influence of muscovite on the thermal transformations of kaolinite from room temperature up to 1,100 °C, *J. Mater. Sci.* 42 (2007) 8745–8752, <https://doi.org/10.1007/s10853-006-0192-7>.
- [45] S. Salem, A. Salem, Mechanisms of momentum transport in viscous flow sintering, *Sinter. Appl.* (2013), <https://doi.org/10.5772/53259>.